*J. Braz. Chem. Soc.*, Vol. 23, No. 3, 555-564, 2012.
Printed in Brazil - ©2012 Sociedade Brasileira de Química
0103 - 5053 $6.00+0.00

Article

# Development of Plurimetallic Electrocatalysts Prepared by Decomposition of Polymeric Precursors for EtOH/$O_2$ Fuel Cell

***Lívia M. Palma, Thiago S. Almeida and Adalgisa R. de Andrade****

*Departamento de Química, Faculdade de Filosofia, Ciências e Letras de Ribeirão Preto, Universidade de São Paulo, Av. Bandeirantes, 3900, 14040-901 Ribeirão Preto-SP, Brazil*

Este trabalho teve como objetivo desenvolver eletrocatalisadores plurimetálicos contendo Pt, Ru, Ni e Sn suportados em C pelo método de decomposição de precursores poliméricos (DPP), na razão metal:carbono de 40:60% em massa, para aplicação em célula a combustível de etanol direta (DEFC). As nanopartículas obtidas foram caracterizadas físico-quimicamente por difração de raios X (DRX) e energia dispersiva de raios X. Os resultados de DRX revelaram cristalitos com estrutura cúbica de face centrada da Pt com evidências de que os átomos de Ni, Ru e Sn foram incorporados à estrutura da Pt. A caracterização eletroquímica das nanopartículas foi realizada por voltametria cíclica e cronoamperometria em meio ácido ($H_2SO_4$ 0,05 mol $L^{-1}$), na ausência e presença de etanol. A adição de Sn para os catalisadores PtRuNi/C deslocou significativamente o potencial de início de oxidação de etanol e CO para valores mais baixos, aumentando assim a atividade catalítica, especialmente para a composição $Pt_{64}Sn_{15}Ru_{13}Ni_8$/C. Eletrólises de solução de etanol em 0,4 V *vs.* ERH permitiram a determinação de acetaldeído e ácido acético como principais produtos da reação. A presença de Ru nas ligas favoreceu a formação de ácido acético como produto principal da oxidação do etanol. O catalisador $Pt_{64}Sn_{15}Ru_{13}Ni_8$/C exibiu o melhor desempenho para DEFC.

This work aimed to develop plurimetallic electrocatalysts composed of Pt, Ru, Ni, and Sn supported on C by decomposition of polymeric precursors (DPP), at a constant metal:carbon ratio of 40:60 wt.%, for application in direct ethanol fuel cell (DEFC). The obtained nanoparticles were physico-chemically characterized by X-ray diffraction (XRD) and energy dispersive X-ray spectroscopy (EDX). XRD results revealed a face-centered cubic crystalline Pt with evidence that Ni, Ru, and Sn atoms were incorporated into the Pt structure. Electrochemical characterization of the nanoparticles was accomplished by cyclic voltammetry (CV) and chronoamperometry (CA) in slightly acidic medium (0.05 mol $L^{-1}$ $H_2SO_4$), in the absence and presence of ethanol. Addition of Sn to PtRuNi/C catalysts significantly shifted the ethanol and CO onset potentials toward lower values, thus increasing the catalytic activity, especially for the quaternary composition $Pt_{64}Sn_{15}Ru_{13}Ni_8$/C. Electrolysis of ethanol solutions at 0.4 V *vs.* RHE allowed determination of acetaldehyde and acetic acid as the main reaction products. The presence of Ru in alloys promoted formation of acetic acid as the main product of ethanol oxidation. The $Pt_{64}Sn_{15}Ru_{13}Ni_8$/C catalyst displayed the best performance for DEFC.

**Keywords**: DEFC, ethanol, decomposition of polymeric precursor method (DPP), metallic catalyst

## Introduction

The development of clean technologies for power generation with renewable fuels is required if we are to overcome the increase in environmental problems. In this context, the use of ethanol as fuel is promising because it is renewable, easy to store and handle, and contains high energy density (8 kW h $kg^{-1}$), which makes it a good candidate to replace traditional oil fuels.[1] In recent years, Brazil has increased its production of ethanol, which has led to growing interest on the part of researches in using this fuel.[2]

In this sense, research involving direct ethanol fuel cell (DEFC) is advantageous. To increase cell efficiency and reduce the limiting effects, it is necessary to find catalysts that promote the complete oxidation of ethanol, *i.e.*, catalyst that can cleave the C–C bond of the ethanol

*e-mail: ardandra@ffclrp.usp.br

molecule, thereby culminating in $CO_2$ formation. However, this does not happen very often,[3] because intermediates that adsorb onto the electrode are formed instead. As a result, the catalytically active sites are poisoned hence decreasing the amount of produced energy. It is frequently reported that the species generated from the oxidation of ethanol are acetic acid, acetaldehyde, and $CO_2$. According to Iwasita and Pastor,[4] the reaction pathways are proportional to the initial concentration of ethanol in solution. The complete oxidation of ethanol to $CO_2$ furnishes 12 electrons (8 kW h $kg^{-1}$), whereas its partial oxidation to acetic acid affords one third of this value (2.67 kW h $kg^{-1}$). Ethanol oxidation to acetaldehyde yields only 1.33 kW h $kg^{-1}$.

Pt catalysts have been widely investigated for the electro-oxidation of fuels such as methanol and ethanol.[4-6] Ethanol is strongly adsorbed onto the platinum surface, which shifts the onset of oxidation potential to higher values, *e.g.*, E > 0.8 V *vs.* RHE. In recent studies Kutz *et al.*[7] using vibrational sum-frequency generation spectroscopy (SFG) found evidences that CO can be formed at lower potentials through fragments of $CH_x$ and $CH_xO$ oxidation indicating C–C bond breaking. Although the experimental conditions for cell operation is much different from the one employed in spectroscopic investigation one cannot discharge this findings. Nevertheless, it is well known that alloys including elements such as Sn, Ru, Ni, Co, Rh, Pd, and W, among others in the platinum structure are much more efficient materials in terms of ethanol oxidation at lower potentials (E < 0.4 V *vs.* RHE).[8-11] This outstanding characteristic is explained by two different effects, namely the bifunctional[12,13] and electronic or binder effects.[14-16]

The bifunctional effect, first described by Watanabe and Motoo,[12,13] ocurrs when elements less noble than Pt and with high affinity for water molecules, such as Ru, easily form oxygen or hydrated oxides species next to a Pt site onto which the organic intermediate is adsorbed. The electronic effect or binder is identified when one metal present in the alloy can change the chemical properties of the first layer of Pt atoms on the catalysts surface, thereby lowering the electronic density at the Fermi level. Alternatively, the metal can partially fill the Pt 5d-orbital, thus decreasing the chemisorption energy of CO intermediates. The better performance of the catalysts that act by this effect is attributed to the fact that electron donation weakens the binding energy of the Pt–C bond; hence favoring oxidation of organic byproducts. As a consequence, the number of free Pt sites for adsorption and oxidation of molecules is increased.[14-16]

Neto *et al.*[17] have described that introduction of Ru into Pt-based catalysts enhances the reactivity towards oxidation and moderates the poisoning effect through formation of meta-stable intermediates, via the bifunctional mechanism. Sn catalysts can electronically modify the electron in the d bands of Pt by changing the adsorption energy. In addition, materials that have Ni in the presence of Ru and/or Sn have furnished promising results regarding the ethanol oxidation in DEFC.[10,18-21]

Camara *et al.*[22] has conducted FTIR studies on PtRu and showed that the amount of acetic acid produced is related to the amount of Ru in the catalyst, *i.e.*, the larger the amount of Ru in the electrocatalyst, the higher the formation of acetic acid and the lower the production of acetaldehyde during ethanol oxidation.

Literature is controversial concerning the selectivity toward acetic acid and acetaldehyde formation during ethanol oxidation on PtSn/C and PtSnRu/C electrocatalysts. After 5 h of electrolysis, Simões *et al.*[23] have observed formation of acetic acid, acetaldehyde, and $CO_2$ in the presence of PtSn electrocatalysts, as attended by HPLC and FTIR analysis. Acetaldehyde was the main product identified in this case. On the other hand, Purgato *et al.*[24] have found that the PtSn/C electrocatalyst favors acetic acid formation, as previously reported by Rousseau *et al.*[6] for PtSn/C and PtSnRu/C electrocatalysts. In another recent investigation, we have noted that PtRuSn/C, prepared by the DPP method, shifts the onset potential for ethanol electrooxidation to 0.20 V *vs.* RHE, acetaldehyde being the main electrolysis product. Moreover, addition of Ru and Sn to Pt has been found to improve the ethanol oxidation rate.[8]

Almeida *et al.*[25] have shown that addition of Ni to PtSn/C catalysts prepared by the DPP method significantly decrease the onset potential of ethanol and CO oxidation, because of a combination between the electronic effect of this metal and the bifunctional effect of Sn. These ternary catalysts were not able to cleave the C–C bond, so the main product was acetaldehyde again.

The aim of this work was to prepare a set of electrocatalysts, namely PtRu, PtNi, PtRuNi, and PtSnRuNi, supported on carbon vulcan by the DPP method, apply them in the electro-oxidation of ethanol in a direct fuel cell, and confirm the role played by the various metals in product selectivity.

## Experimental

### Catalysts preparation

The PtRu/C, PtNi/C, PtRuNi/C, and PtSnRuNi/C catalysts were synthesized by decomposition of polymeric precursors (DPP). Before the synthesis, carbon vulcan XC-72 was heated at 400 ºC under $N_2$ atmosphere for 4 h, in order to eliminate the adsorbed species and clean the carbon surface. The Pt, Ru, Sn, and Ni polymeric precursors

(metallic resins) were prepared separately by mixing citric acid (CA) (Merck) and ethylene glycol (EG) (Merck) at 60-65 °C. After complete dissolution of CA, the temperature was raised to 90 °C, and the metal precursor ($H_2PtCl_6$, $RuCl_3 \cdot nH_2O$, or $NiCl_2 \cdot 6H_2O$), all purchased from Aldrich, or $C_6H_5O_7Sn_2$, synthesized using $SnCl_2$ acquired from Aldrich was added, as described previously.[26] The reaction solution was kept under magnetic stirring for 2-3 h. The metal/CA/EG molar ratio was 1:4:16 for all the polymeric precursors. The nanocatalysts were obtained by mixing the appropriate amount of metallic resins with 5.0 mL ethanol, to obtain the following desired nominal compositions: PtRu (80:20), PtNi (80:20), PtRuNi (70:15:15, 80:10:10), and PtSnRuNi (80:10:5:5). Enough carbon vulcan XC-72 powder was added to the mixture, so that 40 wt.% metal loading would be achieved. Finally, the mixture was homogenized in ultrasonic bath and heated using a temperature program similar to the one described previously.[24] Briefly, the samples were heated under $N_2$ flux (0.05 L $min^{-1}$) to 250 °C at a rate of 1 °C $min^{-1}$ and were kept at this temperature for 60 min. Then, the temperature was raised to 350 °C at a rate of 10 °C $min^{-1}$ and kept there for 120 min.

### Physical and chemical characterization

The diffraction patterns of the catalysts were obtained on an X-ray diffractometer (D5005 Siemens) operating with CuKa radiation ($\lambda$ =1.5406 Å) generated at 40 kV and 40 mA. The following parameters were kept constant during the analysis: 2$\theta$ range = 20°-90°, step = 0.03°, and total analysis time = 1.97 h. Catalyst phase composition and analysis of the position relative to the $K\alpha_1$ monochromatic radiation were obtained by fitting the experimental angular range of interest to the pseudo-Voigt function *per* crystalline peak with the aid of the Profile Plus Executable refinement program (Siemens AG). The crystallite size values were obtained using the Debye-Scherrer equation[27]

$$D = \frac{K(\lambda \times \frac{180^\circ}{\pi})}{\sqrt{(\beta^2 - S^2)}\cos\theta_\beta}$$

where D is the apparent crystallite size, K is the geometric factor (0.9 for spherical crystallite), $\lambda$ is the wavelength of the radiation (1.5406 Å), S is the instrument line broadening (0.001°), $\beta$ is the reflection width at half-maximum intensity (FWHM), and $\theta_\beta$ is the angle corresponding to the maximum intensity of the peak.

The unit cell parameters were determined by a computer program (U-Fit.exe v1.3-1992) using the least-squares method. The 2$\theta$ experimental values and the reflection planes (hkl) were employed for calculation of the unit cell.

Energy dispersive X-ray (EDX) analysis using a Leica microscope Zeiss LEO 440 model TEM coupled to an Oxford 7060 model analyzer was utilized for determination of the composition of the nanocatalysts particles.

### Electrochemical measurements

To perform the electrochemical measurements, 2.0 mg of the electrocatalyst powder were dispersed into a solution (100 µL) consisting of ethanol (95 µL) and Nafion® (5 µL) (5 wt.% in aliphatic alcohols, Aldrich). The mixture was homogenized in ultrasonic bath for 30 min. After homogenization, 20 µL of the suspension were deposited onto a vitreous carbon ($\varnothing$ = 3 mm) previously polished with alumina, which was then followed by drying in an oven at 80 °C for 5 min. The electrochemical measurements were carried out in a conventional three-electrode electrochemical cell (50 mL) using an Autolab (PGSTAT-30) potentiostat Ag/AgCl and a spiralized platinum wire (15 cm) were used as reference and counter electrode, respectively, and all the potentials were converted to the reversible hydrogen electrode (RHE).

The activity of the electrocatalysts was investigated by cyclic voltammetry (potential range of 0.05 to 1.00 V *vs.* RHE) and chronoamperometry (0.4 V *vs.* RHE for 30, 60 and 90 min). The concentrations of the supporting electrolyte ($H_2SO_4$, Merck) and ethanol (Merck) were kept constant at 0.05 mol $L^{-1}$ and 1.0 mol $L^{-1}$, respectively. The electrochemically active area of the electrocatalysts was determined by the CO-stripping technique, which involved oxidation of a monolayer of CO adsorbed on the electrode to $CO_2$, as described elsewhere.[28]

### Electrolysis of ethanol and chromatographic analysis of the reaction products

Electrolysis experiments (0.4 V *vs.* RHE for 12 h) were performed in an electrochemical cell with separate compartments for the cathode and the anode. To increase the anode area for electrolysis, the catalytic ink was deposited on a 2 $cm^2$ carbon-cloth (HT1400W, ELAT® GDL - BASF). The reaction products were analyzed by means of a high performance liquid chromatography (HPLC) apparatus from Shimadzu containing both a UV-Vis (SPD-10A) and a refractive index (RID) detector RID-10A placed in series. The products were separated by an Aminex HPX-87H column (Bio-Rad) operating under isocratic conditions using 3.33 mmol $L^{-1}$ $H_2SO_4$ and a flow rate of 0.6 mL $min^{-1}$. After electrolysis, $N_2$ was bubbled through the solution, to quantify the volatile compounds produced during the process in separate trap compartments. Acetaldehyde was

trapped in a 0.2 wt.% 2,4-dinitrophenyl-hydrazine (200 mL) solution in 2.0 mol $L^{-1}$ HCl. Subsequently, the concentration of the solid hydrazone formed therein was quantified after dissolution in ethyl acetate, using an $NH_2P$-50 (Asanhipak $NH_2P$ series) column by isocratic elution using a mobile phase consisting of acetonitrile/$H_2O$ (40:60 v/v) at a 0.6 mL $min^{-1}$ flow rate. The released $CO_2$ was trapped in 0.1 mol $L^{-1}$ NaOH (2.0 mL). The possibly formed carbonate was quantitatively analyzed by comparison with a $Na_2CO_3$ reference obtained under the same conditions. All the solutions were prepared using Milli-Q water® (18.2 MW cm at 20 °C). The electrolytic solution was thoroughly purged with nitrogen before the electrochemical measurements.

### Preparation of the catalysts and the membrane/electrode assemblies (MEAs)

The membrane electrode assemblies (MEAs) were prepared by hot pressing a pretreated Nafion® 117 membrane placed between an E-TEK cathode (2 mg $cm^{-2}$ metal loading 40 wt.%) and a homemade anode (2 mg $cm^{-2}$ metal loading 40 wt.%) at 130 °C for 90 s, under a pressure of 35 kg $cm^{-2}$. The electrode fabrication procedure has been described elsewhere.[29] The operating fuel cell performances were assessed in a single DEFC with 5.29 $cm^2$ electrode geometric surface area using a test bench (eletrocell). The temperature was set at 90 °C for the fuel cell and at 95 °C for the oxygen humidifier. The pressures of ethanol and oxygen were set to 1 and 3 bar, respectively. The concentration of ethanol was 2 mol $L^{-1}$. The $E_{cell}$ *versus* j and power density *versus* j curves were recorded.

## Results and Discussion

### Physico-chemical characterization of the electrocatalysts

EDX results for all the prepared catalysts are summarized in Table 1. It can be observed that each metal is present in amounts close to the nominal composition in the case of the binary catalysts. However, ternary and quaternary compositions showed major departures from the nominal values. Therefore, the experimental values will be employed to designate the electrocatalyst sample hereafter. This result confirms the data from our previous work[8,9,23,25] showing that DPP is an efficient method for the preparation of nanocatalysts to be applied in ethanol oxidation.

Figure 1 depicts the XRD patterns of carbon-supported Pt-M nanocatalysts. Highly intense narrow peaks can be observed, attesting to the good crystallinity of the materials. The crystallographic planes for pure Pt[30] are represented by dashed lines in Figure 1. The electrocatalysts exhibit the peaks typical of face-centered cubic (fcc / Fm-3m) crystalline Pt and refer to the reflection planes (111), (200), (220), (311), and (222). There is no evidence of formation of other phases derived from introduction of the Ni, Ru, and Sn metals. However, the presence of small amounts of $RuO_2$, $NiO_2$, NiO, NiPt, $SnO_2$ and $Pt_3Sn$ cannot be ruled out, and these would be present in the form of very small crystallites or as an amorphous phase.

There is a small shift to higher 2θ values with respect to pure Pt in the case of the binary and ternary catalyst, an indication of alloy formation. According to the literature,[7] this shift is due the difference in the atomic radii of the metallic elements present in the alloy. For instance, Ru and Ni have smaller atomic radius (Ru = 134 pm, Ni =124 pm) as compared to Pt (138.5 pm).[31] The smaller elements (Ru and Ni) can, in principle, be inserted more easily into the crystalline structure of Pt, thereby favoring alloy formation. When this occurs, the crystalline structure contracts and the XRD reflection planes shift to higher 2θ values.

There are no shifts in the case of the $Pt_{64}Sn_{15}Ru_{13}Ni_8/C$ catalyst as compared to pure Pt. Considering that Sn atoms are larger (151 pm),[31] when Sn is introduced to form the Pt-Sn alloy it promotes a behavior opposite to the one described above for Ru and Ni. In fact, Sn is expected to prompt expansion of the Pt crystalline structure, which should shift the reflection planes toward lower 2θ values. This result has been observed by us for some PtSn/C

**Table 1.** XRD and EDX results for different Pt-M/C nanocatalysts prepared by the DPP process at 350 ºC, under $N_2$ atmosphere

| Eletrocatalysts | | a / Å | V / Å | D / nm | | | | |
|---|---|---|---|---|---|---|---|---|
| Nominal | Experimental* | | | (111) | (200) | (220) | (311) | (222) |
| $Pt_{80}Ni_{20}/C$ | $Pt_{73}Ni_{27}/C$ | 3.907 | 59.65 | 10.67 | 7.43 | 7.58 | 7.77 | 10.37 |
| $Pt_{80}Ru_{20}/C$ | $Pt_{73}Ru_{27}/C$ | 3.914 | 59.95 | 13.92 | 12.44 | 12.10 | 12.55 | 15.55 |
| $Pt_{80}Ru_{10}Ni_{10}/C$ | $Pt_{54}Ru_{29}Ni_{17}/C$ | 3.912 | 59.87 | 13.23 | 12.48 | 14.57 | 12.37 | 12.70 |
| $Pt_{70}Ru_{15}Ni_{15}/C$ | $Pt_{45}Ru_{33}Ni_{22}/C$ | 3.912 | 59.88 | 12.26 | 10.40 | 9.99 | 8.50 | 14.77 |
| $Pt_{80}Sn_{10}Ru_5Ni_5/C$ | $Pt_{64}Sn_{15}Ru_{13}Ni_8/C$ | 3.922 | 60.34 | 14.51 | 12.09 | 11.48 | 10.83 | 13.68 |

*Experimental data obtained by EDX.

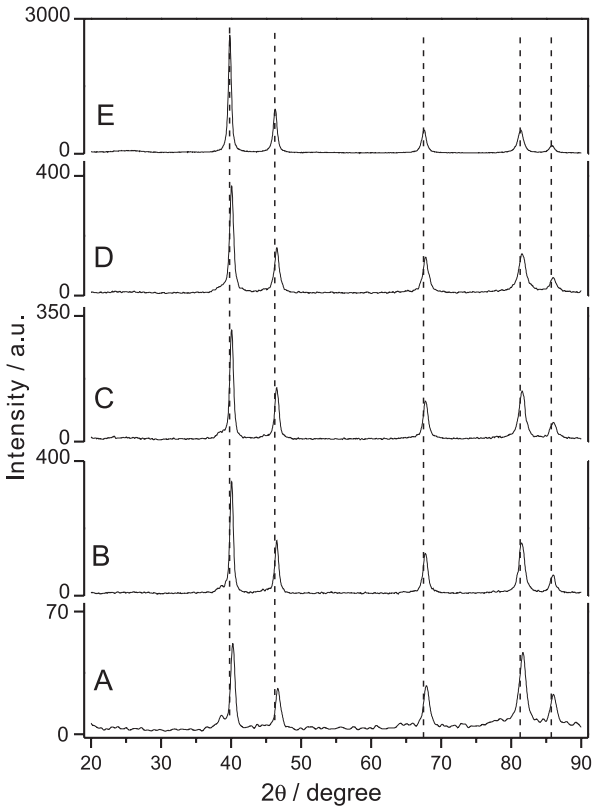


**Figure 1.** XRD patterns of the Pt-M nanoelectrocatalysts prepared by the DPP process and dispersed on carbon vulcan XC-72 (40% wt. metal loading). (A) $Pt_{73}Ni_{27}$/C, (B) $Pt_{73}Ru_{27}$/C, (C) $Pt_{54}Ru_{29}Ni_{17}$/C, (D) $Pt_{45}Ru_{33}Ni_{22}$/C, and (E) $Pt_{64}Sn_{15}Ru_{13}Ni_{8}$/C, (- - -) 2θ value of pure Pt.[30]

catalysts.[9,25] In our opinion, the good matches between the patterns of the quaternary catalyst and pure Pt crystallites are due the opposite effects that Ru, Ni, and Sn have on the crystal structure. Displacement of the crystallographic planes, indicating alloy formation, have also been observed for some PtRuNi/C electrocatalysts prepared by Park,[10] Wang,[19] Liang,[21] and Moreno[32] via different synthetic routes. Taking into account the XRD pattern, one can infer that the preparation of nanocatalysts by DPP suggest Sn, Ru, and Ni incorporation into the Pt crystallite, with consequent alloy formation.

Table 1 displays the lattice parameter and cell volume for the set of nanoelectrocatalysts prepared here. The reported values for the lattice parameter and cell volume of pure Pt are 3.923 Å and 60.38 Å,[3] respectively.[30] The experimental values obtained for the binary and ternary nanoelectrocatalysts are lower than those of pure Pt. This indicates formation of an alloy which is in accordance with Vegard's Law.[16,33] However, as explained before, the introduction of Sn into $Pt_{64}Sn_{15}Ru_{13}Ni_{8}$/C does not elicit any shifts as compared to pure Pt.

The crystallite sizes, obtained by means of Debye-Scherrer's equation,[27] are in the 7.40-22.50 nm range. The great difference observed among the different reflection planes attest to the high heterogeneity of the particles formed by the DPP method. For comparison with other electrocatalysts prepared by the same method, the (220) reflection plane was chosen. It can be noticed that the crystallite size of the Pt-M nanocatalysts prepared here are in the same order of magnitude as others reported recently by one of us, *e.g.*, PtSnW/C - 7.8 nm,[8] PtSnIr/C - 8 nm,[34] PtRuSn/C - 5.1 nm,[9] and PtSnNi/C - 5.1 nm.[25] Smaller crystallite sizes can be obtained for similar metallic compositions when the preparation method is changed. For instance, chemical reduction using the sodium borohydride furnishes PtRuNi/C electrocatalysts with a crystallite size of 4.4 nm (the authors considered the diffraction peak (111) for calculation of D-values).[19] Smaller PtRuNi crystallite sizes, with average values of 3.3 nm, have been obtained by means of the colloidal and microemulsion methods.[18,20,21] Liang *et al.*[21] have produced even smaller PtRuNi nanoelectrocatalysts (2-3 nm) by using the microwave heating method. Although the values reported for the DPP method are higher than the ones described in the literature, several studies have demonstrated that rearrangement of the nanoparticles might occur during operation under fuel cell conditions (high temperature and pressure).[8,34]

## Electrochemical measurements

Figure 2A illustrates some representative cyclic voltammograms obtained for the nanoelectrocatalysts prepared by the DPP method in 0.05 mol $L^{-1}$ $H_2SO_4$. The region comprised between 0.05 and 0.40 V *vs.* RHE is characteristic of hydrogen adsorption/desorption at Pt sites. Introduction of transition metals suppresses the hydrogen adsorption peaks, as reported before.[16,35] Another noteworthy fact is the low acidity of the supporting electrolyte employed herein (0.05 mol $L^{-1}$), which is 10 times lower than the one commonly used during classic fuel cell investigation (0.50 mol $L^{-1}$). This low concentration of ionized hydrogen can also diminish the hydrogen adsorption peak.

The region between 0.40 and 0.85 V *vs.* RHE includes the electrical double layer, as well as the capacitive and pseudo-capacitive currents, a result of the oxidation and reduction of solid-state species. Comparing the charges obtained for this region with those reported for binary, ternary, and quaternary nanoelectrocatalysts in the literature,[16,35-37] it is evident that nanoelectrocatalysts containing Ru exhibit higher voltammetric charge. Explanations for the increased charge in the double layer region are the presence of a larger number of molecules for activation/deactivation of water molecules and the pseudo-capacitive process. According to Baranova *et al.*,[38] the low current density observed in the

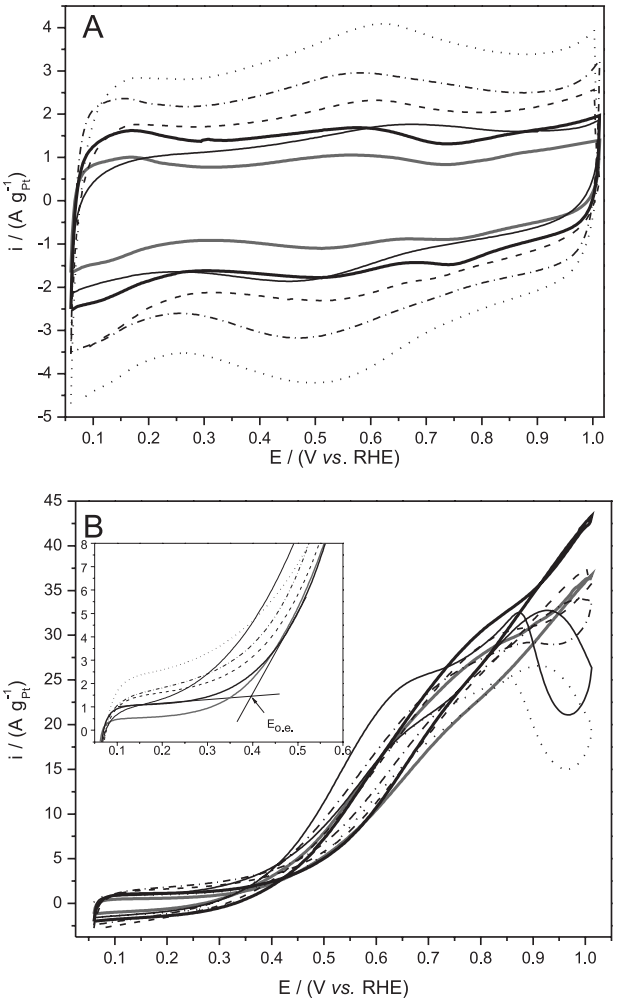


**Figure 2.** Cyclic voltammograms of the Pt-M/C nanoelectrocatalysts at 10 mV $s^{-1}$ in the absence (A) and presence (B) of ethanol (1.0 mol $L^{-1}$). (▬) Pt/C, (▬)$Pt_{73}Ni_{27}$/C; (- - -) $Pt_{73}Ru_{27}$/C,(···) $Pt_{54}Ru_{29}Ni_{17}$/C, (-·-·-) $Pt_{45}Ru_{33}Ni_{22}$/C, and (——)$Pt_{64}Sn_{15}Ru_{13}Ni_8$/C. Supporting electrolyte = 0.05 mol $L^{-1}$ $H_2SO_4$; A = 0.07 $cm^2$. Current values normalized according to the Pt loading. (Inset: onset potential for ethanol electro-oxidation).

cyclic voltammograms of PtSn/C catalysts can be attributed to alloys with a disordered structure. In the case of the $Pt_{64}Sn_{15}Ru_{13}Ni_8$/C nanoelectrocatalyst, this can account for the low double layer current.

Above 0.80 V *vs.* RHE, there is a rise in the current, which is ascribed to the formation/reduction of Pt-containing species.[35]

Figure 2B brings the cyclic voltammograms obtained for the different nanoelectrocatalysts prepared here in the presence of 1 mol $L^{-1}$ ethanol. It can be verified that the changes observed in the supporting electrolyte are suppressed in the presence of ethanol.

Although literature describes that the introduction of Ru and Ni into the Pt-based nanocatalyst shifts the onset potential of methanol oxidation in highly acidid medium,[10,18,32] the onset potential for ethanol oxidation for binary and ternary nanoelectrocatalysts prepared by the DPP method remains almost the same as compared to Pt/C. In fact, Wang *et al.*[19] have reported an onset potential for ethanol oxidation in the case of the PtRuNi/C nanoelectrocatalyst prepared by the sodium borohydride method similar to the values found in this study. The same feature has been reported by Ribadeneira and Hoyos.[20] All these results confirm the actual knowledge that the best nanoelectrocatalyst alloy for DMFC must contain Ru, which is responsible for attenuating the oxidation overpotential.[10,18,32] On the other hand, it is well known that one must introduce Sn into the Pt-based alloy in order to obtain the same positive effect on ethanol oxidation.[39,40]

Therefore, introducing Sn into the alloy shifts the onset potential of ethanol oxidation to less positive values, *i.e.*, around 0.4 V *vs.* RHE. Table 2 list the best results obtained for ethanol electro-oxidation.

Figure 3 displays the current *vs.* time curves obtained at 0.4 V *vs.* RHE for ethanol oxidation in the presence of the Pt-M nanoelectrocatalysts. The main feature of these curves has been discussed before.[8,34] Briefly, at 0.4 V *vs.* RHE, ethanol molecules adsorb onto the nanocatalyst sites, which were previously covered by water molecules. Dissociation may occur after adsorption, thereby producing strongly adsorbed CO and $CH_x$ species or other C–C intermediates. This event is responsible for a sudden drop in the current during the experiment, once

**Table 2.** Catalytic performance of the nanoelectrocatalysts prepared herein for ethanol oxidation as a function of the electrode material

| Nanoelectrocatalysts | $E_{o.e.}$ / V *vs.* RHE | $E_{co}$ / V *vs.* RHE | Mass activity / (A $g_{Pt}^{-1}$) | | | EAA* / ($m^2$ $g_{Pt}^{-1}$) | Intrinsic activity / (mA $m^{-2}$) |
|---|---|---|---|---|---|---|---|
| | | | 30 min | 60 min | 90 min | | |
| Pt/C | 0.449 | 0.303 | 1.69 | 1.40 | 1.30 | 7.88 | 214 |
| $Pt_{73}Ni_{27}$/C | 0.477 | 0.258 | 1.14 | 1.06 | 0.87 | 9.32 | 157 |
| $Pt_{73}Ru_{27}$/C | 0.479 | 0.287 | 1.49 | 1.09 | 0.98 | 9.21 | 123 |
| $Pt_{54}Ru_{29}Ni_{17}$/C | 0.511 | 0.257 | 1.19 | 0.92 | 0.76 | 6.94 | 98 |
| $Pt_{45}Ru_{33}Ni_{22}$/C | 0.465 | 0.311 | 1.46 | 1.17 | 1.02 | 13.33 | 109 |
| $Pt_{64}Sn_{15}Ru_{13}Ni_8$/C | 0.397 | 0.287 | 3.05 | 2.23 | 1.74 | 5.25 | 582 |

*EAA = electrochemically active area.

the number of active sites is drastically reduced due to the surface poisoning.[41]

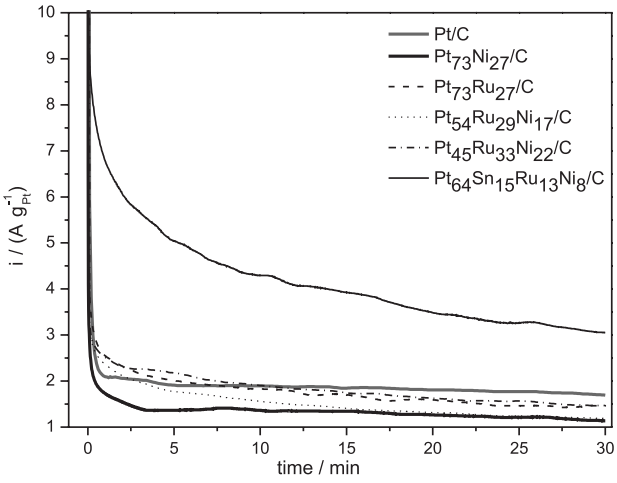


**Figure 3.** Current *vs.* time plots for the electro-oxidation of 1 mol $L^{-1}$ ethanol in mildly acidic medium (0.05 mol $L^{-1}$) at 0.4 V *vs.* RHE on the as prepared Pt-M/C nanoelectrocatalysts. Current values normalized by Pt loading.

The best catalytic activity was obtained for the quaternary nanoelectrocatalyst $Pt_{64}Sn_{15}Ru_{13}Ni_8/C$. It is well known that Ru and Sn are oxophilic, and that Sn and Ni modify the surface through an electronic mechanism.[10,19] Thus, the good results achieved for the quaternary nanoelectrocatalysts can be ascribed to improved synergism among the metals introduced into the Pt-M alloy. Introduction of a fourth element (Ni) into the Pt-Sn-Ru/C nanoelectrocatalyst promoted activation of adsorption sites and enhanced oxidation of the fuel and/or its intermediates as compared to PtRuNi/C prepared here. When these data are compared to recent results obtained in our laboratory for ternary PtSnNi/C[25] and PtSnRu/C[9] we observed that the quaternary nanoelectrocatalyst offers similar catalytic activity. However, the outstanding value obtained for PtSnNi/C,[25] 15 A $g_{Pt}^{-1}$, must be attributed not only to changes in the composition of the catalyst but also to a better distribution of the active sites due to the small changes made to the route employed for preparation of the alloy adopted in the latter investigation.

In order to determine the stability of the nanoelectrocatalysts, three successive chronoamperometry were performed as shown in Table 2, the decrease in the activity of the $Pt_{64}Sn_{15}Ru_{13}Ni_8/C$ nanoeletrocatalyst is smaller as compared to the other investigated compositions, indicating that regeneration of the active sites is higher for this plurimetallic nanoelectrocatalyst. Table 2 denotes that the mass activity decreases for all the catalysts independently of the presence of Ni indicating that a relatively good stability of Ni in the investigated medium. So it can be concluded that introduction of the three metals into the Pt-based nanoelectrocatalyst is beneficial and reflects on a better stability.

The onset potential of CO oxidation for the PtSnRu/C nanoelectrocatalysts studied by Cunha *et al.*[9] was larger than the ones obtained here (Table 2). This can be due to nickel inclusion which modifies the electronic structures of Pt, thereby reducing the potential of CO oxidation on its surface. This is corroborated by the work of Almeida *et al.*,[25] where the values obtained for the PtSnNi/C nanoelectrocatalysts lay between 0.244 and 0.274 V *vs.* RHE.

The electrochemically active area (EAA) of the nanoelectrocatalysts, presented in Table 2 was calculated by estimating the oxidation of a CO monolayer. The default value for a smooth polycrystalline platinum monolayer loading is 420 mC $cm^{-2}$ ($Q_{CO}^{0}$).[28] In order to compare the different Pt-M nanoelectrocatalysts loadings, the EAA values were normalized by the amount of platinum that was employed. The $Pt_{45}Ru_{33}Ni_{22}/C$ nanoelectrocatalysts gave the highest EAA (13.33 $m^2 g_{Pt}^{-1}$), whilst the quaternary nanocatalyst yielded the lowest value (5.25 $m^2 g_{Pt}^{-1}$). This astonishing result can be understood by taking into account the relationship between EAA and particle size, as reported before by many research groups.[38,42-44] Thus, different types of adsorption occur within the surface of the nanocatalysts. Larger particles with rough surface allied with irregular clusters should have different energy for CO adsorption as compared to nanoparticles.

The intrinsic catalytic activity (mA $m^{-2}$) was calculated by using the EAA (Table 2). The quaternary nanoelectrocatalyst displayed the highest intrinsic catalytic activity, thereby confirming the catalytic activity results.

### Ethanol electrolysis

Table 3 presents the results obtained for ethanol (1.0 mol $L^{-1}$) electrolyses at a fixed potential (0.4 V *vs.* RHE). The percentage of ethanol conversion at the binary and ternary nanoelectrocatalysts containing Ru is larger as compared to the other nanoelectrocatalysts. This confirms our previous results[25] and shows the dependence of material consumption on the nanoelectrocatalyst composition.

The large range of average mass balance (60-90%) is due to the long time of the electrolysis experiments (12 h) and is mainly related to the high volatility of the formed product ($CO_2$, acetaldehyde) at room temperature.

All the nanoelectrocatalysts led to formation of acetic acid and acetaldehyde as the main products of ethanol oxidation. Generation of traces of $CO_2$ cannot be ruled out, as verified from the HPLC data in the range of the limit

**Table 3.** Ethanol oxidation as a function of the plurimettalic nanoelectrocatalysts*

| Electrocatalyst | % Ethanol consumed | Acetic acid / (mmol $L^{-1}$) | Acetaldehyde / (mmol $L^{-1}$) | Mass balance / % |
|---|---|---|---|---|
| $Pt_{73}Ni_{27}/C$ | 7.4 | 3.2 | 66.8 | 89.4 |
| $Pt_{73}Ru_{27}/C$ | 29.1 | 195.2 | 71.6 | 80.5 |
| $Pt_{54}Ru_{29}Ni_{17}/C$ | 24.7 | 138.7 | 108.5 | 79.0 |
| $Pt_{45}Ru_{33}Ni_{22}/C$ | 22.9 | 154.5 | 58.6 | 61.6 |
| $Pt_{64}Sn_{15}Ru_{13}Ni_{8}/C$ | 6.7 | 1.2 | 57.4 | 90.5 |

*$H_2SO_4$ 0.5 mol $L^{-1}$, ethanol 1.0 mol $L^{-1}$, T = 22 ºC.

of quantification of the technique. The amount of acetic acid obtained in the case of the $Pt_{73}Ru_{27}/C$, $Pt_{54}Ru_{29}Ni_{17}/C$, and $Pt_{45}Ru_{33}Ni_{22}/C$ nanoelectrocatalysts is higher than the quantity of acetaldehyde. These electrocatalysts contain a similar amount of Ru in their composition. This behavior is in agreement with the work of Camara *et al.*,[22] based on FTIR-data reporting that the amount of generated acetic acid increases as the Ru content is raised in the binary Pt/PtRu catalysts. In other words, higher percentages of Ru (over 30%) promote enhanced selectivity toward acetic acid production. It is important to notice that we are investigating the effect of both ruthenium concentration and pH on the final product selectivity. This is because in a previous electrolysis ran in more acidid medium (0.2 mol $L^{-1}$ $H_2SO_4$) we obtained acetaldehyde as the main product for $Pt_xSn_yRu_z/C$ catalysts when z was maintained below 10%.[9]

The fact that $Pt_{73}Ni_{27}/C$ and $Pt_{64}Sn_{15}Ru_{13}Ni_{8}/C$ favored acetaldehyde formation confirms that the presence of Sn and Ni promotes increased yields of acetaldehyde.[25] The low consumption of ethanol observed for the quaternary catalyst is in contrast with other electrochemical data, published in the literature,[6,8,9,23,25] and can be assigned to the heterogeneous distribution of the metals on the surface of the nanoelectrocatalyst. The nanoparticles can dissolve and re-cristalize which contributes to inhindance their activity under drastic conditions. In fact, it is difficult to compare literature data once composition, distribution, and experimental conditions differ from one laboratory to another.[6,18,20,32,40]

## Fuel cell performance

Figure 4 gives the cell performance at 90 °C. The open circuit potential of the cell for $Pt_{64}Sn_{15}Ru_{13}Ni_{8}/C$ was 0.71 V, but all the other electrocatalysts furnished values below this one. The power density of the cell obtained for the quaternary electrocatalyst was 11 mW $cm^{-2}$, while for the others it did not exceed 5 mW $cm^{-2}$. This data is in line with the chronoamperometric experiments. Our results are in the same order of magnitude as those obtained for one PtRuNi/C electrocatalysts prepared by the alcohol reduction method, where power density ranges close to 4 mW $cm^{-2}$ were achieved.[20] The cell results also confirm the current knowledge that Sn-atoms is essential for enhancement of the power capacity of DEFCs.[8,34,39] However, the maximum value obtained here is lower than the value generally reported in the literature for similar catalysts (*ca.* 30 mW $cm^{-2}$).[3,8,34] Comparing absolute power density values among laboratories is a difficult task, but the results presented in Figure 4 which were obtained in the same experimental conditions,

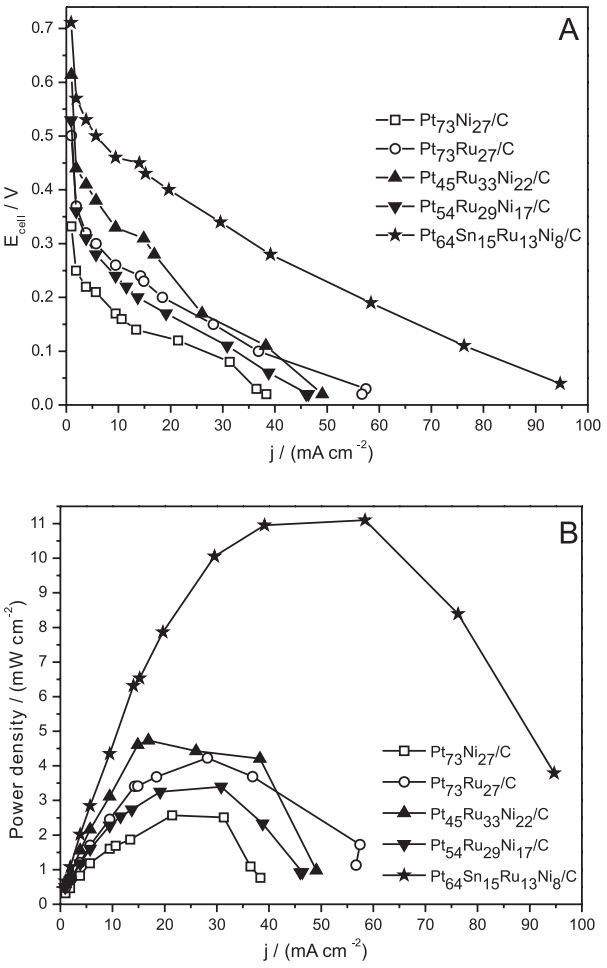


**Figure 4.** Cell voltage (V) (A) and power density (mW $cm^{-2}$) (B) *versus* current density (mA $cm^{-2}$) obtained in a single direct ethanol fuel cell at 90 ºC using plurimetallic Pt-M catalysts. (2 mg $cm^{-2}$ electrocatalyst loading, 40 wt.% electrocatalyst on carbon). $P(O_2)$ = 3 bar; P(EtOH) = 1 bar; [EtOH] = 2.0 mol $L^{-1}$; Nafion® 117 membrane.

*i.e.*, similar MEAs preparation, and equipment operating conditions, we can eliminate experimental variations from the final value. So it can be concluded that Sn has a positive effect on ethanol conversion.

## Conclusions

Plurimetallic nanoelectrocatalysts containing Pt, Ru, Sn, and Ni supported on carbon prepared by the DPP method display Pt face centered cubic (fcc) structure and there is alloy formation with no phase segregation of the embedded metals. The crystallite sizes range from 7.4 to 22.5 nm, considering the reflection plane (220). The onset potential of ethanol oxidation is switched to lower values upon Sn introduction, suggesting improvement in the electrocatalyst performance. The longterm electrolysis confirms that the presence of high percentages of Ru (over 30%) promotes acetic acid production. The single DEFC test confirms cyclic voltammograms and chronoamperometry results showing that the $Pt_{64}Sn_{15}Ru_{13}Ni_8$/C electrocatalyst is more active for ethanol oxidation thus furnishing higher power density values. In conclusion, Sn has a positive effect on the ethanol conversion.

## Acknowledgments

The authors acknowledge CAPES, FAPESP and CNPq for the financial support.

## References

1. Lamy, C.; Lima, A.; Lerhun, V.; Delime, F.; Coutanceau, C.; Léger, J.-M.; *J. Power Sources* **2002**, *105*, 283.
2. http://www.brasil.gov.br acessed in January 2011.
3. Vigier, F.; Rousseau, S.; Coutanceau, C.; Léger, J.-M.; Lamy, C.; *Top. Catal.* **2006**, *40*, 111.
4. Iwasita, T.; Pastor, E.; *Electrochim. Acta* **1994**, *39*, 531.
5. Hitmi, H.; Belgsir, E. M.; Léger, J.-M.; Lamy, C.; Lezna, R. O.; *Electrochim. Acta* **1994**, *39*, 407.
6. Rousseau, S.; Coutanceau, C.; Lamy, C.; Léger, J.-M.; *J. Power Sources* **2006**, *158*, 18.
7. Kutz, R. B.; Braunschweig, B.; Mukherjee, P.; Behrens, R. L.; Dlott, D. D.; Wieckowski, A.; *J. Catal.* **2011**, *278*, 181.
8. Ribeiro, J.; Dos Anjos, D. M.; Léger, J.-M.; Hahn, F.; Olivi, P.; De Andrade, A. R.; Tremiliosi-Filho, G.; Kokoh, K. B.; *J. Appl. Electrochem.* **2008**, *38*, 653.
9. Cunha, E. M.; Ribeiro, J.; Kokoh, K. B.; De Andrade, A. R.; *Int. J. Hydrogen Energy* **2011**, *36*, 11034.
10. Park, K.; Choi, J.; Kwon, B.; Lee, S.; Sung, Y.-E.; Ha, H.-Y.; Hong, S.-A.; Kim, H.; Wieckowski, A.; *J. Phys. Chem. B* **2002**, *106,* 1869.
11. Xiong, L.; Kannan, A. M.; Manthiram, A.; *Electrochem. Commun.* **2002**, *4,* 898.
12. Watanabe, M.; Motoo, S.; *J. Electroanal. Chem.* **1975**, *60,* 267.
13. Watanabe, M.; Motoo, S.; *J. Electroanal. Chem.* **1975**, *60,* 275.
14. Igarashi, H.; Fujino, T.; Zhu, Y. M.; Uchida, H.; Watanabe, M.; *Phys. Chem. Chem. Phys.* **2001**, *3,* 306.
15. Goodenough, J. B.; Manoharan, R.; Shukla, A. K.; Ramesh, K. V.; *Chem. Mater.* **1989**, *1*, 391.
16. Li, H.; Sun, Cao, G. L.; Jiang, L.; Xin, Q.; *Electrochim. Acta* **2007**, *52,* 6622.
17. Neto, A. O.; Giz, M. J.; Perez, J.; Ticianelli, E. A.; Gonzalez, E. R.; *J. Electrochem. Soc.* **2002**, *149*, A272.
18. Martínez-Huerta, M. V.; Rojas, S.; La Fuente, J. L. G.; Terreros, P.; Peña, M. A.; Fierro, J. L. G.; *Appl. Catal., B* **2006**, *69*, 75.
19. Wang, Z.; Yin, G.; Zhang, J.; Sun, Y.; Shi, P.; *J. Power Sources* **2006**, *160*, 37.
20. Ribadeneira, E.; Hoyos, B. A.; *J. Power Sources* **2008**, *180,* 238.
21. Liang, Y.; Zhang, H.; Tian, Z.; Zhu, X.; Wang, X.; Yi, B.; *J. Phys. Chem. B* **2006**, *110*, 7828.
22. Camara, G. A.; Lima, R. B. De; Iwasita, T.; *Electrochem. Commun.* **2004**, *6*, 812.
23. Simões, F. C.; Dos Anjos, D. M.; Vigier, F.; Léger, J.-M.; Hahna, F.; Coutanceau, C.; Gonzalez, E. R.; Tremiliosi-Filho, G.; De Andrade, A. R.; Olivi, P.; Kokoh, K. B.; *J. Power Sources* **2007**, *167*, 1.
24. Purgato, F. L. S.; Olivi, P.; Léger, J.-M.; De Andrade, A. R.; Tremiliosi-Filho, G.; Gonzalez, E. R.; Lamy, C.; Kokoh, K. B.; *J. Electroanal. Chem.* **2009**, *628*, 81.
25. Almeida, T. S.; Kokoh, K. B.; De Andrade, A. R.; *Int. J. Hydrogen Energy* **2011**, *36*, 3803.
26. Besso, M. M.; *US pat. 3,213,120* **1965**.
27. Cullity, B. D.; *Elements of X-ray Diffraction*, 3th ed., Addison-Wesley: San Francisco, 1978.
28. Vidakovic, T.; Christov, M.; Sundmacher, K.; *Electrochim. Acta* **2007**, *52*, 5606.
29. Léger, J.-M.; Rousseau, S.; Coutanceau, C.; Hahn, F.; Lamy, C.; *Electrochim. Acta* **2005**, *50*, 5118.
30. Powder Diffraction File PDF-2: 00-004-0802; *Joint Committee on Powder Diffraction Standards*, International Center for Diffraction Data: Pennsylvania, USA, 2005.
31. Dean, J. A.; *Lange's Handbook of Chemistry*, 14th ed., R, R, Donnelly & Sons Company: USA, 1992.
32. Moreno, B.; Chinarro, E.; Pérez, J. C.; Jurado, J. R.; *Appl. Catal., B* **2007**, *76*, 368.
33. Jacob, K. T.; Raj, S.; Rannesh, L.; *Int. J. Mater. Res.* **2007**, *98*, 776.
34. Ribeiro, J.; Dos Anjos, D. M.; Kokoh, K. B.; Olivi, P.; Coutanceau, C.; Léger, J. -M.; De Andrade, A. R.; Tremiliosi-Filho, G.; *Electrochim. Acta* **2007**, *52*, 6997.
35. Ciapina, E. G.; Gonzalez, E. R.; *J. Electroanal. Chem.* **2009**, *626*, 130.

36. Calegaro, M. L.; Suffredini, H. B.; Machado, S. A. S.; Avaca, L. A.; *J. Power Sources* **2006**, *156*, 300.
37. Profeti, L. P. R.; Simões, F. C.; Olivi, P.; Kokoh, K. B.; Coutanceau, C.; Léger, J.-M.; Lamy, C.; *J. Power Sources* **2006**, *158*, 1195.
38. Baranova, E. A.; Amir, T.; Mercier, P. H. J.; Patarachau, B.; Wang, D.; Page, T. L.; *J. Appl. Electrochem.* **2010**, *40*, 1767.
39. Ermete, A.; *J. Power Sources* **2007**, *170*, 1.
40. Neto, A. O.; Dias, R. R.; Tusi, M. M.; Linardi, M.; Spinacé, E. V.; *J. Power Sources* **2007**, *166*, 87.
41. Xia, X. H.; Liess, H.-D.; Iwasita, T.; *J. Electroanal. Chem.* **1997**, *437*, 233.
42. Pozio, A.; Francesco, M.; Cemmi, A.; Cardellini, F.; Giorgi, L.; *J. Power Sources* **2002**, *105*, 13.
43. Camara, G. A.; Giz, M. J.; Paganin, V. A.; Ticianelli, E. A.; *J. Electroanal. Chem.* **2002**, *537*, 21.
44. Arenz, M.; Mayrhofer, K. J. J.; Stamenkovic, V.; Blizanac, B. B.; Tomoyuki, T.; Ross, P. N.; Markovic, N. M.; *J. Am. Chem. Soc.* **2005**, *127*, 6819.

*Submitted: October 19, 2011*
*Published online: January 31, 2012*

**FAPESP has sponsored the publication of this article.**